Investigating the Structural, Functional, and Biochemical Properties of PP_i-dependent PEPCK Paralogs from *Entamoeba histolytica*

By Siddhi Balamurali
Department of Biological Sciences and Statistics, College of Agriculture and Life Sciences

Abstract

Phosphoenolpyruvate carboxykinase (PEPCK) is an important metabolic enzyme which functions to interconvert oxaloacetic acid (OAA) and phosphoenolpyruvate (PEP) in the Krebs cycle, a key process of generating cellular energy. There exist three known classes of PEPCK - two of which are nucleotide-dependent, using ATP and GTP. Very little is known about the third, PP_i-dependent PEPCK. Comparing classes, nucleotide-dependent PEPCKs are both functionally and structurally similar (~60-70 kDa) whereas PP_i-dependent PEPCK bears significant functional and structural differences (~130 kDa). This presented work investigates PP_i-dependent PEPCK from a human parasite *Entamoeba histolytica* (*Eh*PEPCK). It is unique from previous work done on another homolog from *Propionibacterium freudenreichii* (*Pf*PEPCK) in that there are three paralogs instead of one. This suggests increased complexity in function and regulation. This work has determined that the interaction between *Eh*PEPCK paralogs gives rise to dimers and heterotrimers, and certain interactions show substrate induced inhibition. Kinetic measurements were completed to determine the metal cofactor of *Eh*PEPCKs, and to determine the kinetic consequences of the aforementioned oligomeric states. The experiments support the conclusion that aggregation causes substrate inhibition, and that dimers are more active than trimers.

Introduction

Phosphoenolpyruvate carboxykinase (PEPCK) is an important metabolic enzyme suggested to be the master regulator of TCA cycle flux (Yang et al., 2009). It operates by removing citric acid cycle anions to be used in other metabolic processes, namely gluconeogenesis, glyceroneogenesis, 1-carbon serine synthesis, or works to replenish the TCA cycle (Yang et al., 2009). PEPCK has implications in glucose-stimulated insulin secretion (a process in diabetes), senescence, tuberculosis, and in cancer and has been thought of as a potential therapeutic target (Jeon et al., 2015; Mendez-Lucas et al., 2014; Montal et al., 2015; Park et al., 2014; Marrero et al., 2010; Yuan et al., 2016; Santra et al., 2016; Yang et al., 2009b). The PEPCK family has classically been divided into two nucleotide-dependent classes: those which utilized ATP, and those that utilized GTP as a phosphoryl donor. *In vivo*, PEPCK is thought to primarily catalyzes the reaction in which oxaloacetic acid (OAA) is converted into phosphoenolpyruvate (PEP) and carbon dioxide using its nucleotide substrate (McLeod and Holyoak, 2021). However *in vitro*, PEPCK can complete the reverse reaction as well, making them bidirectional. More recently, a third PEPCK which utilizes pyrophosphate (PP_i) was discovered, further expanding the family. The two nucleotide-dependent PEPCKs are well characterized in both their structure and function. PEPCK requires two cation metal cofactors for activity, named M1 and M2 (Willard et al., 1969). M1 is an active site cofactor which binds to the enzyme and bridges the substrate and nucleotide binding pockets. M2 binds as a nucleotide-metal complex (McLeod and Holyoak, 2021). In the nucleotide-dependent PEPCKs, the chemical reaction is most activated when the M1 metal is Mn^{2+} and

the M2 metal is Mg^{2+} (Das et al., 2012; Machova et al., 2015; Hebda and Nowak, 1982; Hidalgo et al., 2016; Sokaribo et al., 2020; Escos et al., 2016; Wilkes et al., 1982). The active site of the enzyme contains three important loops (Fig.1). The P-loop binds the nucleotide and positions it correctly for phosphoryl transfer (Matte et al., 1996). The R-loop binds the substrates (OAA/PEP) and once bound, moves to allow closure of the Ω-loop (Holyoak et al., 2006). Finally, the Ω-loop acts as a gate/lid and protectively encloses the active site while the reaction takes place (Johnson and Holyoak, 2010).

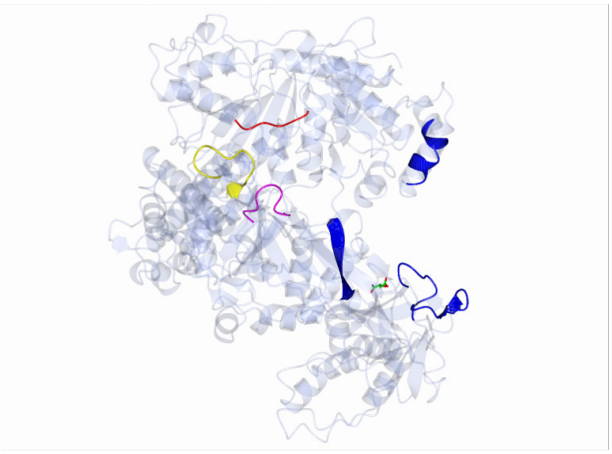

Figure 1. Structure of PPi-dependent PfPEPCK. The P-loop (magenta), R-loop (red), and Ω-loop are shown along with the dimer interface (blue).

Initial studies on the PP_i-dependent class of PEPCK were completed in the 1960s and 1970s (Siu et al., 1961; Lochmuller et al., 1966; Willard and Rose, 1973; O'Brien et al., 1973; Wood et al., 1969; Haberland et al., 1972) In these studies, PP_i-dependent PEPCK from *Propionibacterium freudenreichii* (*Pf*PEPCK) was evaluated. These studies were then re-evaluated to determine the differences between the nucleotide and pyrophosphate using classes (McLeod and Holyoak, 2021). First, PP_i-dependent PEPCKs are approximately twice the size (~130kDa) of nucleotide-dependent PEPCKs (~70kDa), with a mostly conserved (in relation to nucleotide-dependent PEPCKs) core structure including the active site residues/loops (Fig.1). However, this extra mass has manifested as additional "lobes" around this conserved core. Second, *Pf*PEPCKs preferentially use Fe^{2+} as the M1 cofactor instead of Mn^{2+}. Third, although ATP- and GTP-dependent PEPCKs preferentially catalyzed the OAA→PEP reaction, PP_i-dependent PEPCK favors the PEP→OAA reaction (Lochmuller et al., 1966). Fourth, PPi-dependent PEPCK exhibits substrate inhibition where high concentrations of PEP lead to inactivation, whereas ATP- and GTP-dependent PEPCKs do not. Finally, in this substrate-induced inactivated state, the enzyme oligomerizes from monomers to homodimers. In addition to substrate (PEP or OAA), malate was shown to bind to an allosteric site which presumably causes this dimerization. In contrast, nucleotide-dependent PEPCKs are typically monomeric and have not been observed to have any regulation by ligand-induced quaternary structure changes (Fukuda et al., 2004).

The PP_i-dependent class has been relatively understudied despite *Pf*PEPCK having unique characteristics when compared to nucleotide-dependent PEPCKs. A new isozyme of PP_i-dependent PEPCK from *Entamoeba histolytica* (*Eh*PEPCK) was previously studied (McLeod and Holyoak, 2021). *Entamoeba histolytica* is a human parasite and studying it may provide a therapeutic avenue to target this organism (Chou and Austin, 2022). Deeper insight into the structure and function may help to discover how to selectively target this enzyme. In the Chiba et al. study, a unique trimer was observed (McLeod and Holyoak, 2021). However, there was no understanding as to what oligomeric states are possible, how these oligomeric states arise (ligand-induce or paralog interactions), or the paralog/oligomer activities. Here, I structurally and functionally characterize these three isoforms in isolation and in combination to understand these structure-function relationships.

Structural characterization was completed using small angle X-ray scattering (SAXS). SAXS uses X-ray scattering to determine low-resolution structural details on macromolecules. Specifically, structural information that can be obtained are: the radius of gyration (R_g) (mean distance from the center of mass or central axis to the outer edges), estimated molecular

weight, the D_{max} (is the maximum dimension of the molecule), and low-resolution shape information (ie. long rod vs sphere). Further analysis of structural information yields scattering curves and Kratky plots. Kratky plots qualitatively determine the flexibility and degree of unfolding in the sample. Dimensionless Kratky plots normalize scattering profiles by mass and concentration (Hopkins et al., 2017). An unfolded protein displays a plateau with a high q, while globular proteins display a bell shaped curve, and a combination of the two may show characteristics of both. As the oligomerization of *Eh*PEPCK will lead to large changes in size, SAXS accurately assessed the oligomerization states of the paralogs. SAXS data was collected both with and without substrates and known effectors of *Pf*PEPCK to determine how the addition of substrates affects oligomerization state. In addition to structural characterization, kinetic experiments were done to map functional consequences to given structures. Prior to full kinetic measurements, the optimal metal cofactor (M1) was determined as this was shown to be variable between classes. The activity of each paralog in isolation, and in combination was measured (work ongoing). These experiments have revealed a general mechanism of substrate regulation of *Eh*PEPCKs which can then be compared to *Pf*PEPCK to determine similarities and differences.

Materials and Methods

PP_i, PEP, and NADH were purchased from ChemImpex. BME was purchased from Sigma Aldrich. MDH was purchased from Calzyme Laboratories. HEPES was obtained from Gold Biotechnology. Sodium Bicarbonate was purchased from Mallinckrodt Pharmaceuticals. The enzyme was purified previously at Cornell University after recombinant expression. All other chemicals were purchased from the highest grade available.

Small Angle X-ray Scattering of *Eh*PEPCK paralogs (SAXS)

SAXS was used to determine the oligomeric states of *Eh*PEPCKs in isolation, in combination and with different ligands. Screening for optimal conditions was performed using a BioXolver (Xenocs) home-source instrument at Cornell's Laboratory of Atomic and Solid-State Physics. The data was recollected at Sector 7A1 (BioSAXS) at the Cornell High Energy Synchrotron Source (CHESS) to extend signal/noise and resolution limits (Table 1). Final samples were in 50 mM TRIS pH 8.0 and 2 mM TCEP at a final volume of 20 uL and the total concentration of *Eh*PEPCK was 1.25 mg/mL.

Table 1. CHESS SAXS collection parameter details for EhPEPCK structural studies.

Wavelength (Å)	1.103
Detector distance (cm)	1735
Exposure number/sample	10
Exposure length (s)	1
Q range ($Å^{-1}$)	0.000123 - 0.577

Paralog activity measurements using Michaelis-Menten Kinetics

$$PEP + P_i + CO_2 \rightarrow OAA + PP_i$$

The kinetic constants were determined for the paralog *Eh*1, and the combinations *Eh*1+2 and *Eh*1+3 of *Entamoeba histolytica*, with experimentation in progress for every paralog and combination possible for the three paralogs. The assays were done in duplicate at room temperature at a final volume of 1 mL. A Varian 50 Bio UV-Visible Spectrophotometer was used to monitor enzyme activity. The conversion of PEP to OAA in each assay was monitored at 340 nm via a coupled reaction using malate dehydrogenases by observing the change of NADH to NAD^+. An R script from McLeod and Holyoak (2021) was used to determine Michaelis-Menten parameters by fitting data to the substrate inhibition model (Eq. 1)

$$\frac{Vmax * \text{substrate concentration}}{(Km + \text{substrate concentration}) * (1 + (\text{substrate concentration} / Ki))}$$

Equation 1

The standard assay mix for PEP carboxylation was composed of 100 mM HEPES pH 7.5, 20 mM BME, 300 μM NADH, 10 mM KH_2PO_4,

5 mM $MgCl_2$, 250 µM $MnCl_2$ (or other M1 metal substitute), 40 mM $KHCO_3$ (bubbled with dry ice), PEP varying from 2.5 uM to 10,000 uM, 5U of malate dehydrogenase (MDH) and 5 µg of PP_i-dependent PEPCK (*Eh*1, *Eh*2, or *Eh*3). Reactions were initiated with the addition of PP_i-dependent PEPCK. To determine what metal is used most effectively as a cofactor by *Eh*PEPCK, kinetic assays with *Eh*1 were performed with each one using 250 µM of the following metals: iron ($FeCl_3$), manganese ($MnCl_2$), magnesium ($MgCl_2$), calcium ($CaCl_2$), zinc ($ZnCl_2$), copper ($CuCl_2$), and cobalt ($CoCl_2$). As zinc and copper did significantly react in the initial round of testing, they both were not included in final testing, and therefore are not included in the discussion.

Results and Discussion

Paralog oligomerization determined by SAXS

Small-angle x-ray scattering (SAXS) uses X-rays to determine low resolution structural details on macromolecules. SAXS was used here to determine the quaternary state of the paralogs in isolation (*Eh*1, *Eh*2, and *Eh*3) and in combination (*Eh*1+2, *Eh*1+3, *Eh*2+3, *Eh*1+2+3), both with and without substrate (both OAA and PEP) as well as a known allosteric effector of *Pf*PEPCK (malate) (Table 2). It was observed that in isolation, all three paralogs have approximately the same D_{max} values of 140, 139, and 142 Å (respectively) and R_g values of 47.1, 44.2, and 48.4 Å (Table 2). They also have the near identical scattering curves, Kratky plots, and P(r) functions (Fig.2). *Eh*2+3 is approximately the same as the paralogs in isolation, with an R_g of 45.6 Å and D_{max} of 139 Å. The dimer structure from crystallized *Pf*PEPCK was found to have an R_g of 46.4 Å and D_{max} of 139 Å (Manalastas-Cantos et al., 2021). Hence, *Eh*1, 2, 3, and *Eh*2+3's R_g and D_{max} values are, without the addition of substrate or ligand, suggestive of a dimer complex. It is unknown if *Eh*2 and *Eh*3 combine to form a heterodimer, or if they are only present as homodimers.

Table 2. D_{max} and R_g values of Eh1, 2, and 3 in isolation and in combination.

***Eh*PEPCK**	**1**	**2**	**3**	**1+2**	**1+3**	**2+3**	**1+2+3**
D_{max} (Å)	140	139	142	192	192	139	195
R_g (Å)	47.1 ± 0.277	44.2 ± 0.379	48.4 ± 0.358	66.1 ± 0.618	62.4 ± 0.568	45.6 ± 0.381	61.4 ± 0.187
10 mM PEP	**1**	**2**	**3**	**1+2**	**1+3**	**2+3**	**1+2+3**
D_{max} (Å)	Agg.*	160	165	Agg.*	Agg.*	150	480
R_g (Å)	Agg. *	53.5 ± 0.511	53 ± 0.673	Agg.*	Agg.*	56.2 ± 0.607	120.6 ± 1.18
10mM OAA	**1**	**2**	**3**	**1+2**	**1+3**	**2+3**	**1+2+3**
D_{max} (Å)	Agg.*	175	155	Agg.*	Agg.*	150	235
R_g (Å)	Agg.*	57.3 ± 0.694	51.7 ± 0.378	Agg.*	Agg.*	49.1 ± 0.374	72.2 ± 0.257
40 mM Malate	**1**	**2**	**3**	**1+2**	**1+3**	**2+3**	**1+2+3**
D_{max} (Å)	139	144	145	255	250	145	250
R_g (Å)	53.3 ± 0.503	46.5 ± 0.357	48.2 ± 0.373	65.6 ± 0.882	68.6 ± 1.65	45.7 ± 0.304	72.1 ± 0.274

*Aggregation

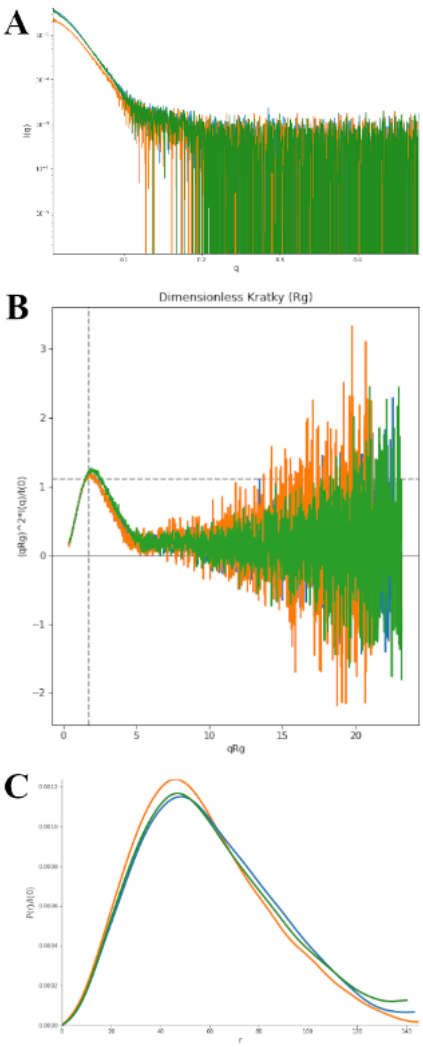

Figure 2. ***Eh*1, *Eh*2, and *Eh*3 in isolation form dimeric structure.** SAXS scattering profiles indicate that each paralog in isolation is the same dimeric structure (when compared to theoretical R_g/D_{max} of known dimeric structure). A) Scattering Curve of *Eh*1 (blue), *Eh2* (orange) and *Eh3* (green). B) Normalized Kratky Plot. C) Normalized P(r).

To determine the molecular origins of the previously reported trimer (McLeod and Holyoak, 2021), each combination was tested. In combination *Eh*1+2, 1+3, and 1+2+3 have approximately the same D_{max} (192, 192, and 195 Å) and R_g (66.1, 62.4, and 61.4 Å) values, which are higher than the aforementioned paralogs in isolation (or *Eh*2+3) (Table 2). This suggests that this complex is a heterotrimer as opposed to *Eh*1 forming a homotrimer with itself as *Eh*2 or 3 is also required to form this structure. Comparing *Eh*1 (dimer) with *Eh*1+2 (trimer), there is a clear change in the structure as observed by the scattering curve (Fig. 3) which is the same structure as *Eh*1+2+3 (Fig. 4). At a sequence level, both *Eh*2 and *Eh*3 share 98% sequence similarity with one another, whereas they only share 90% sequence similarity with *Eh*1. It is therefore not surprising that *Eh*1, being most unique of the three, is the required component for the heterotrimer species.

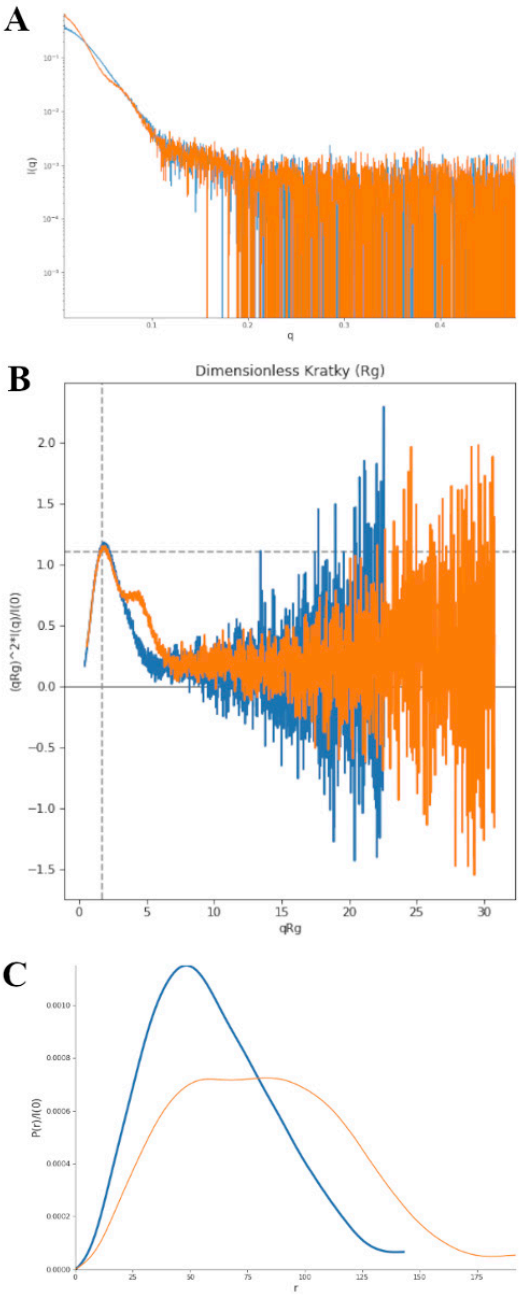

Figure 3. *Eh*1 in isolation forms a dimeric structure, while *Eh*1+2 forms a trimeric structure. *Eh*1 SAXS curve shows the characteristic dimeric scattering curve whereas *Eh*1+2 shows different scatter of the proposed trimeric state. A) SAXS scattering curve of Eh1 in isolation (blue) and with *Eh*1+2 (orange). B) Normalized Kratky plot. C) Normalized P(r).

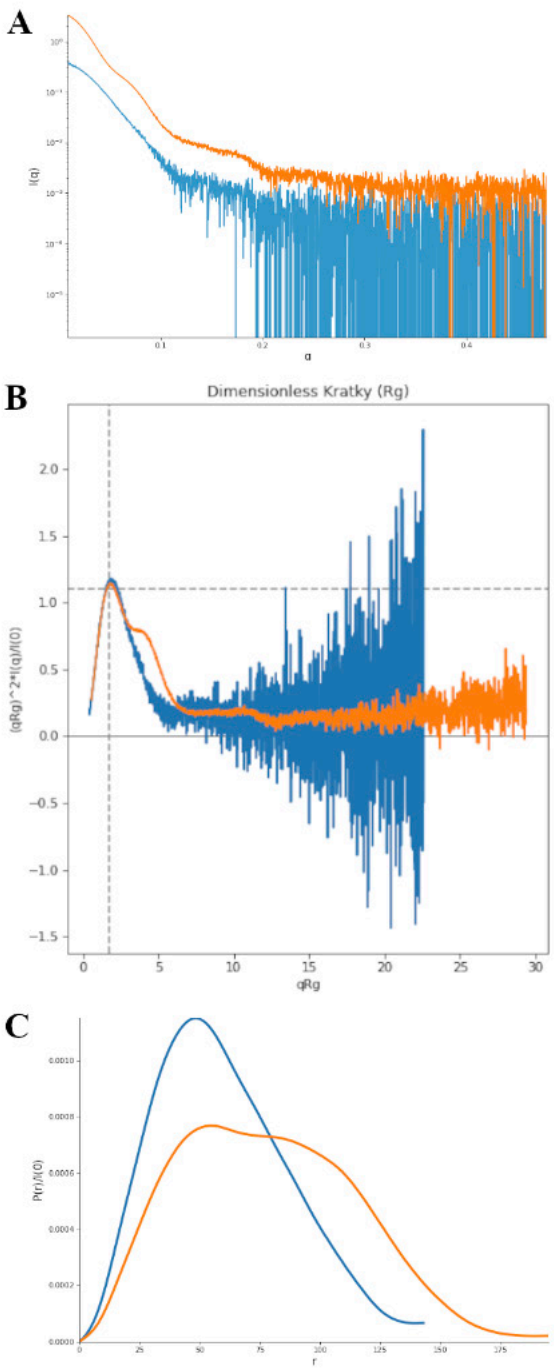

Figure 4. Eh1 in isolation forms a dimeric structure, while Eh1+2+3 forms a trimeric structure. *Eh*1 SAXS curve shows the characteristic dimeric scattering curve whereas *Eh*1+2+3 shows a differing scatter indicative of the trimeric state A) Scattering Curve of *Eh*1 (blue) and *Eh*1+2+3 (orange). B) Normalized Kratky plot. C) Normalized P(r).

Effector molecules induced changes in structure

When substrates or effector molecules bind to their partners, they can often induce structural changes. *Pf*PEPCK for instance, formed a homodimer upon binding of PEP, OAA, and malate (unpublished). Similar experiments were completed here to determine the effect of substrates and malate on *Eh*PEPCK structure. It was found that the effect of OAA and PEP were identical. First, when PEP is present with *Eh*2, *Eh*3 or both *Eh*2+3, an increase in both D_{max} (160, 165, and 150 Å) and R_g (53.5, 53, and 56.2 Å) is observed (Table 2). This suggests that the addition of PEP causes a larger structure to form. However, it is unclear what this structure is. The aforementioned values are greater than the known dimer dimensions, but less than a trimer's, so it could perhaps be an expanded dimer. Second, the addition of 10 mM PEP to *Eh*1, as well as *Eh*1+2 and *Eh*1+3 caused aggregation (the accumulation and/or clumping together of structures) such that the R_g and D_{max} values could not reliably be determined. This suggests that substrates specifically interact with *Eh*1 causes it to destabilize and aggregate, whereas *Eh*2 and *Eh*3 are unaffected. Finally, with *Eh*1+2+3 and 10 mM PEP (only) there is a substantial change compared to the unbound trimer (Fig. 5). This conformational change is evident by all diagnostic plots, and the combination with substrate almost doubles the R_g from 61.4 to 120.6 Å and increases the D_{max} considerably from 195 to 480Å, which points to the probable formation of a much larger structure, whose specifics are unknown but may be a trimer-of-trimers.

The addition of 40 mM malate does not seem to have much effect on the enzyme. In *Eh*1 on, *Eh*2, and *Eh*3, no change was seen in the D_{max} values, which stayed at approximately 140 Å each, which is in contrast to the addition of OAA and PEP, which caused aggregation in *Eh*1. However, an increase in the R_g value of *Eh*1 was seen from 47.1 to 53.3 Å, while *Eh*2 and *Eh*3 saw little to no change. Malate caused a slight increase in size in *Eh*1+2, *Eh*1+3, and *Eh*1+2+3, as the D_{max} values increased from 192, 192, and 195 Å respectively, to 255, 250, and 250 Å. The R_g values for *Eh*1+2, *Eh*1+3, and *Eh*1+2+3 stayed approximately the same, as they changed from 66.1,62.4, and 61.4 Å to 65.6, 68.6. and 72.1 Å respectively.

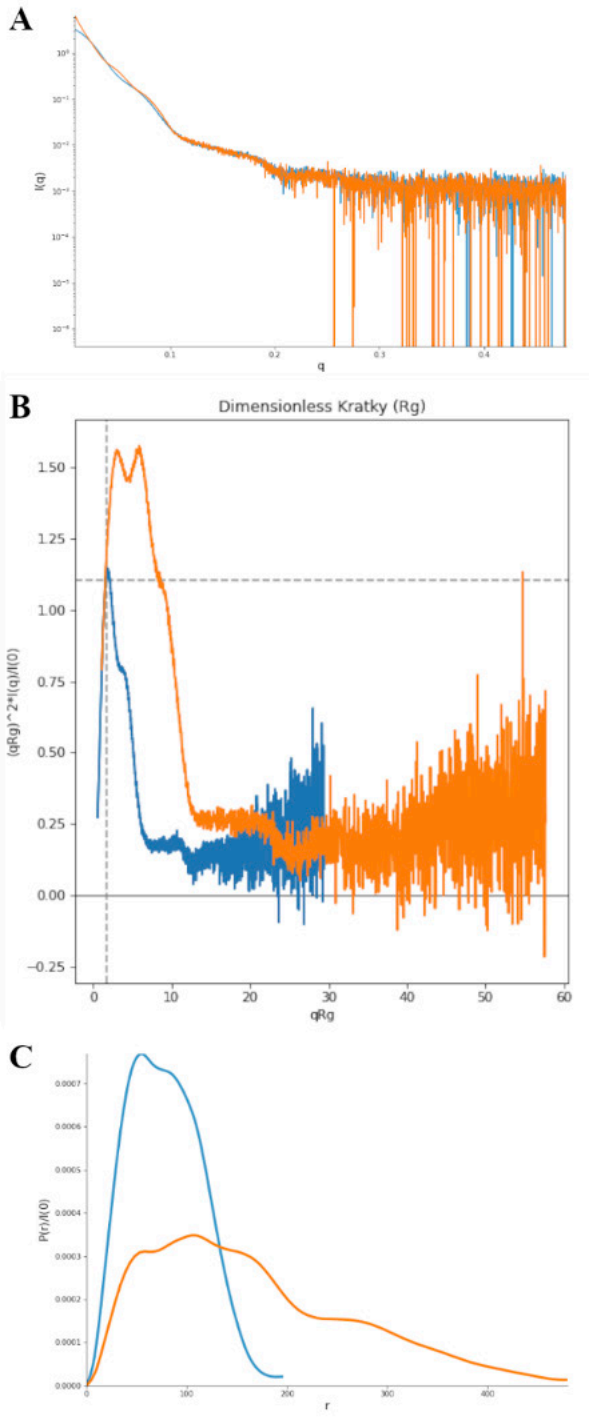

Figure 5. *Eh*1+2+3 forms a proposed trimeric structure, while *Eh*1+2+3 with 10 mM PEP forms an unknown larger structure. A) Scattering Curve *Eh*1+2+3 in isolation (blue) and with 10 mM PEP substrate (orange). B) Normalized Kratky plot. C) Normalized P(r).

Metal Dependency

The SAXS data has revealed the structures of these paralogs both in isolation, and in combination with one another and with the addition of substrate and ligand. However, the activity of these structures is unknown. In order to understand the functionality of each structure, kinetic activity experiments were performed. Before these experiments could be carried out, the optimal conditions for activity had to be determined. Therefore, different metals were tested to see which one functioned as the most activating M1 cofactor. The first experiment done testing metal-dependency to determine if Fe^{2+} is the most activating cation for *Eh*PEPCK as it was in *Pf*PEPCK. Various metals were tested: iron (Fe^{2+}), manganese (Mn^{2+}), magnesium (Mg^{2+}), calcium (Ca^{2+}), and cobalt (Co^{2+}). It was found after testing was complete that manganese was the best M1 Metal cofactor (Table 3).

Activity of *Eh*PEPCK Paralogs

With the optimal metal determined, Michaelis-Menten plots while varying PEP were obtained. *Eh*1 was tested first, and there was an increase in activity at small concentrations of PEP, with the activity gradually decreasing as substrate concentration increases, showing classical substrate inhibition (Fig. 6). The SAXS analysis suggests that *Eh*1 is a dimer in isolation with no evidence of trimer formation but with the addition of PEP, *Eh*1 aggregates suggesting this may be the structural cause of the strong substrate inhibition. Next, *Eh*1+2 and *Eh*1+3 start as a trimer and have stronger substrate inhibition than *Eh*1. Like *Eh*1, aggregation was shown by SAXS and is also likely the origin of the substrate inhibition. Looking at the kinetic constants collected *Eh*1 and *Eh*1+2/1+3 have approximately the same Michaelis-Menten constant (K_M), however, the maximal specific activity of *Eh*1 is over three times greater than that of *Eh*1+2/1+3 (Table 4). While *Eh*1 undergoes substrate inhibition, the determined K_i values suggest that the inhibition is stronger for *Eh*1+2/1+3. Thus, *Eh*1 started as a dimer with higher activity than the trimer, and while both dimer and trimers experienced aggregation with PEP, the trimers appear to be more sensitive.

Table 3. Metal dependency of *Eh*1 PEPCK.

	Fe^{2+}	Mn^{2+}	Mg^{2+}	Co2+	Ca^{2+}
Average rate (µmol/min/mg)	1.59 ±0.10	2.82 ±0.28	2.44 ±0.25	0.050 ±0.03	1.97 ±0.25

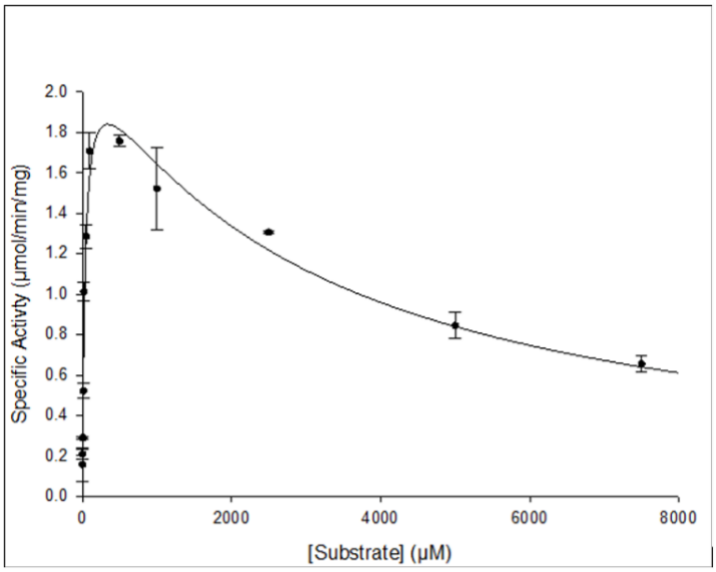

Figure 6. Substrate Inhibition of paralog *Eh*1. *Eh*1's activity was measured with PEP concentration of 2 – 10,000 mM PEP. It undergoes substrate inhibition - Its activity decreases as it undergoes oligomerization.

Table 4. *Eh*PEPCKs and Respective V_{max}, K_m, and K_i values.

*Eh*PEPCK(s)	1	1+2	1+3
V_{max} (µmol/min/mg)	2.3 ± 0.11	0.9 ± 0.14	0.70 ± 0.12
K_m (µM)	39.6 ± 4.8	26.9 ± 8.91	39.5 ± 13.3
K_i (µM)	2960 ± 470	511 ± 166	476 ± 154

Conclusion and Future Directions

Structural analysis showed the oligomerization states of each paralog in isolation and in combination where *Eh*1, *Eh*2 and *Eh*3 are dimers, while *Eh*1+2, *Eh*1+3, and *Eh*1+2+3 exist as heterotrimers. With the addition of substrate, aggregation in *Eh*1, *Eh*1+2, and *Eh*1+3 was observed but not seen in the dimeric complexes and with the trimeric *Eh*1+2+3. Instead, *Eh*1+2+3 formed large structure with over twice the R_g value and 2.5x increase in D_{max} value. Malate did not affect *Eh*2, *Eh*3, or *Eh*2+3. It caused a D_{max} value increase in *Eh*1 and an overall increase in *Eh*1+2, *Eh*1+3, and *Eh*1+2+3, which suggests that it interacts especially with *Eh*1 and its combinations, causing a different, slightly larger trimer to form. These observations are different from what was observed previously in *Pf*PEPCK, which underwent dimerization from the addition of malate, OAA, and PEP, with PEP inducing the least change. SAXS is a useful method, but is low resolution, and prevents the observations of monomers as the high concentrations required force *Eh*PEPCK to dimeric (or trimeric) states. Therefore, the monomer-dimer/trimer transition may also be affected by substrates (or malate). In order to further understand conformational changes, it would be useful to repeat these experiments with crystallography, to observe the exact structures under different conditions.

Kinetically, it was discovered that Mn^{+2} was the most activating M1 cofactor, which is similar to the nucleotide-dependent classes, but

different from *Pf*PEPCK (Fe^{2+}). Of the paralogs tested, *Eh*1 had the highest activity out of *Eh*1, *Eh*1+2, and *Eh*1+3, with over twice the V_{max} of the other two. All three showed activity at low concentrations of PEP but *Eh*1+2/1+3 are most sensitive. From SAXS, this suggests that aggregation is causing substrate inhibition. In order to further understand these paralogs activity, it should be considered to test the kinetic activity of either *Eh*2 or *Eh*3 in isolation. These are both dimers, but do not experience aggregation, and should not suffer substrate inhibition.

Acknowledgements

The kinetic research was completed at the Thorne laboratory at Cornell University's Laboratory of Atomic and Solid-State Physics. The SAXS research was done at Sector 7A1 at Cornell High Energy Synchrotron Source (CHESS), supported by Cornell University.

References

Yang, J., Kalhan, S. C., & Hanson, R. W. (2009a). What is the metabolic role of phosphoenolpyruvate carboxykinase? *Journal of Biological Chemistry, 284*(40), 27025–27029. https://doi.org/10.1074/jbc.r109.040543

Jeon, J. Y., Lee, H., Park, J., Lee, M., Park, S. W., Kim, J. S., Lee, M., Cho, B. C., Kim, K., Choi, A. M., Kim, C. K., & Yun, M. (2015). The regulation of glucose-6-phosphatase and phosphoenolpyruvate carboxykinase by autophagy in low-glycolytic hepatocellular carcinoma cells. *Biochemical and Biophysical Research Communications, 463*(3), 440–446. https://doi.org/10.1016/j.bbrc.2015.05.103

Méndez-Lucas, A., Hyroššová, P., Novellasdemunt, L., Viñals, F., & Perales, J. C. (2014). Mitochondrial phosphoenolpyruvate carboxykinase (PEPCK-M) is a pro-survival, endoplasmic reticulum (ER) stress response gene involved in tumor cell adaptation to nutrient availability. *Journal of Biological Chemistry, 289*(32), 22090–22102. https://doi.org/10.1074/jbc.m114.566927

Montal, E., Dewi, R. E., Bhalla, K., Ou, L., Hwang, B. J., Ropell, A. E., Gordon, C., Liu, W. J., DeBerardinis, R. J., Sudderth, J., Twaddel, W., Boros, L. G., Shroyer, K. R., Duraisamy, S., Drapkin, R., Powers, S., Rohde, J. M., Boxer, M. B., Wong, K., & Girnun, G. D. (2015). PEPCK coordinates the regulation of central carbon metabolism to promote cancer cell growth. *Molecular Cell, 60*(4), 571–583. https://doi.org/10.1016/j.molcel.2015.09.025

Park, J. W., Kim, S. C., Kim, W. K., Hong, J. H., Kim, K., Yeo, H. Y., Lee, J. Y., Kim, M. S., Kim, J. H., Yang, S. Y., Kim, D. Y., Oh, J. H., Cho, J. Y., & Yoo, B. C. (2014). Expression of phosphoenolpyruvate carboxykinase linked to chemoradiation susceptibility of human colon cancer cells. *BMC Cancer, 14*(1). https://doi.org/10.1186/1471-2407-14-160

Marrero, J., Rhee, K. Y., Schnappinger, D., Pethe, K., & Ehrt, S. (2010). Gluconeogenic carbon flow of tricarboxylic acid cycle intermediates is critical for Mycobacterium tuberculosis to establish and maintain infection. *Proceedings of the National Academy of Sciences of the United States of America, 107*(21), 9819–9824. https://doi.org/10.1073/pnas.1000715107

Yuan, Y., Hakimi, P., Kao, C., Kao, A., Liu, R., Janocha, A. J., Boyd-Tressler, A., Hao, X. S., Alhoraibi, H., Slater, E., Xia, K., Cao, P., Shue, Q., Ching, T. T., Hsu, A. L., Erzurum, S. C., Dubyak, G. R., Berger, N. A., Hanson, R. W., & Feng, Z. (2016). Reciprocal Changes in Phosphoenolpyruvate Carboxykinase and Pyruvate Kinase with Age Are a Determinant of Aging in Caenorhabditis elegans. *Journal of Biological Chemistry, 291*(3), 1307–1319. https://doi.org/10.1074/jbc.m115.691766

Santra, S., Cameron, J. M., Shyr, C., Zhang, L., Drögemöller, B. I., Ross, C. J., Wasserman, W. W., Wevers, R. A., Rodenburg, R. J., Gupte, G.,

Preece, M. A., & Van Karnebeek, C. D. (2016). Cytosolic phosphoenolpyruvate carboxykinase deficiency presenting with acute liver failure following gastroenteritis. Molecular Genetics and Metabolism, 118(1), 21–27. https://doi.org/10.1016/j.ymgme.2016.03.001

Yang, J., Kalhan, S. C., & Hanson, R. W. (2009b). What is the metabolic role of phosphoenolpyruvate carboxykinase? *Journal of Biological Chemistry, 284*(40), 27025–27029. https://doi.org/10.1074/jbc.r109.040543

Chiba, Y., Kamikawa, R., Nakada-Tsukui, K., Saito-Nakano, Y., & Nozaki, T. (2015). Discovery of PPI-type phosphoenolpyruvate carboxykinase genes in eukaryotes and bacteria. *Journal of Biological Chemistry, 290*(39), 23960–23970. https://doi.org/10.1074/jbc.m115.672907

McLeod, Matthew J. and Holyoak, Todd. (2021) Phosphoenolpyruvate Carboxykinases. Encyclopedia of Biological Chemistry, 3rd Edition. vol.3, pp.400–412. Oxford:Elsevier.

Das, B., Tandon, V., Saxena, J. K., Joshi, S., & Singh, A. R. (2012). Purification and characterization of phosphoenolpyruvate carboxykinase from *Raillietina echinobothrida*, a cestode parasite of the domestic fowl. *Parasitology, 140*(1), 136–146. https://doi.org/10.1017/s0031182012001254

Machová, I., Snášel, J., Dostál, J., Brynda, J., Fanfrlík, J., Singh, M., Tarábek, J., Vaněk, O., Bednárová, L., & Pichová, I. (2015). Structural and Functional Studies of Phosphoenolpyruvate Carboxykinase from Mycobacterium tuberculosis. *PLOS ONE, 10*(3), e0120682. https://doi.org/10.1371/journal.pone.0120682

Hebda, C., & Nowak, T. (1982). Phosphoenolpyruvate carboxykinase. Mn^{2+} and Mn^{2+} substrate complexes. *Journal of Biological Chemistry, 257*(10), 5515–5522. https://doi.org/10.1016/s0021-9258(19)83807-3

Hidalgo, J., Latorre, P., Carrodeguas, J. A., Velázquez-Campoy, A., Sancho, J., & López-Buesa, P. (2016). Inhibition of Pig phosphoenolpyruvate carboxykinase isoenzymes by 3-Mercaptopicolinic acid and novel inhibitors. *PLOS ONE, 11*(7), e0159002. https://doi.org/10.1371/journal.pone.0159002

Sokaribo, A., Novakovski, B., Cotelesage, J. J. H., White, A. P., Sanders, D., & Goldie, H. (2020). Kinetic and structural analysis of Escherichia coli phosphoenolpyruvate carboxykinase mutants. *Biochimica Et Biophysica Acta - General Subjects, 1864*(4), 129517. https://doi.org/10.1016/j.bbagen.2020.129517

Escós, M., Latorre, P., Hidalgo, J., Hurtado-Guerrero, R., Carrodeguas, J. A., & López-Buesa, P. (2016). Kinetic and functional properties of human mitochondrial phosphoenolpyruvate carboxykinase. *Biochemistry and Biophysics Reports, 7*, 124–129. https://doi.org/10.1016/j.bbrep.2016.06.007

Wilkes, J. M., Cornish, R., & Mettrick, D. F. (1982). Purification and properties of phosphoenolpyruvate carboxykinase from Ascaris suum. *International Journal for Parasitology.* https://doi.org/10.1016/0020-7519(82)90012-1

Matte, A., Goldie, H., Sweet, R. M., & Delbaere, L. T. J. (1996). Crystal Structure of Escherichia coli Phosphoenolpyruvate Carboxykinase: A New Structural Family with the P-loop Nucleoside Triphosphate Hydrolase Fold. *Journal of Molecular Biology, 256*(1), 126–143. https://doi.org/10.1006/jmbi.1996.0072

Holyoak, T., Sullivan, S., & Nowak, T. (2006). Structural Insights into the Mechanism of PEPCK Catalysis,. *Biochemistry, 45*(27), 8254–8263. https://doi.org/10.1021/bi060269g

Johnson, T. A., & Holyoak, T. (2010). Increasing the conformational entropy of the Ω-Loop lid domain in phosphoenolpyruvate carboxykinase impairs catalysis and decreases catalytic fidelity,. *Biochemistry, 49*(25), 5176–5187. https://doi.org/10.1021/bi100399e

Siu, P. M. L., Wood, H. G., & Stjernholm, R. (1961). Fixation of CO2 by phosphoenolpyruvic carboxytransphosphorylase. *Journal of Biological Chemistry, 236*(4), PC21–PC22. https://doi.org/10.1016/s0021-9258(18)64271-1

Lochmüller, H., Wood, H. G., & Davis, J. J. (1966). Phosphoenolpyruvate carboxytransphosphorylase. *Journal of Biological Chemistry, 241*(23), 5678–5691. https://doi.org/10.1016/s0021-9258(18)96398-2

Willard, J. M., & Rose, I. A. (1973). Formation of enolpyruvate in the phosphoenolpyruvate carboxytransphosphorylase reaction. *Biochemistry, 12*(26), 5241–5246. https://doi.org/10.1021/bi00750a003

O'Brien, W. E., Singleton, R., & Wood, H. G. (1973). Carboxytransphosphorylase. VII. Phosphoenolpyruvate carboxytransphosphorylase. Investigation of the mechanism with oxygen-18. *Biochemistry, 12*(26), 5247–5253. https://doi.org/10.1021/bi00750a004

Wood, H. G., Davis, J. J., & Willard, J. M. (1969). Phosphoenolpyruvate carboxytransphosphorylase. V. Mechanism of the reaction and the role of metal ions. *Biochemistry, 8*(8), 3145–3155. https://doi.org/10.1021/bi00836a003

Haberland, M. E., Willard, J. M., & Wood, H. G. (1972). Phosphoenolpyruvate carboxytransphosphorylase. VI.Catalytic and physical structures. *Biochemistry, 11*(5), 712–722. https://doi.org/10.1021/bi00755a007

Chou A., Austin R.L., (2022). Entamoeba Histolytica. In: StatPearls [Internet]. Treasure Island (FL): StatPearls Publishing; 2023 Jan–. PMID: 32491650.

Willard, J. M., Davis, J. J., & Wood, H. G. (1969). Phosphoenolpyruvate carboxytransphosphorylase. IV. Requirement for metal cations. *Biochemistry, 8*(8), 3137–3144. https://doi.org/10.1021/bi00836a002

Fukuda, W., Fukui, T., Atomi, H., & Imanaka, T. (2004). First Characterization of an Archaeal GTP-Dependent Phosphoenolpyruvate Carboxykinase from the Hyperthermophilic Archaeon *Thermococcus kodakaraensis* KOD1. *Journal of Bacteriology, 186*(14), 4620–4627. https://doi.org/10.1128/jb.186.14.4620-4627.2004

J. B. Hopkins, R. E. Gillilan, and S. Skou. Journal of Applied Crystallography (2017). 50, 1545-1553. BioXTAS RAW: improvements to a free open-source program for small-angle X-ray scattering data reduction and analysis. doi: 10.1107/S1600576717011438

Manalastas-Cantos, K., Konarev, P. V., Hajizadeh, N. R., Kikhney, A., Petoukhov, M. V., Molodenskiy, D., Panjkovich, A., Mertens, H. D. T., Gruzinov, A., Borges, C., Jeffries, C. M., Svergun, D. I., & Franke, D. (2021). *ATSAS 3.0*: expanded functionality and new tools for small-angle scattering data analysis. *Journal of Applied Crystallography, 54*(1), 343–355. https://doi.org/10.1107/s1600576720013412